CFD-based methodology for the characterization of the combustion process of a passive pre-chamber gasoline engine

Transportation Engineering 13 (2023) 100200

Contents lists available at ScienceDirect

Transportation Engineering

journal homepage: www.sciencedirect.com/journal/transportation-engineering

Full Length Article

CFD-based methodology for the characterization of the combustion process of a passive pre-chamber gasoline engine

A. Piano [a,*], A. Scalambro [a], F. Millo [a], F. Catapano [b], P. Sementa [b], S. Di Iorio [b], A. Bianco [c]

[a] Politecnico di Torino, Energy Department, Italy
[b] Institute of Sciences and Technologies for Sustainable Energy and Mobility (STEMS), National Research Council, Italy
[c] Powertech Engineering, Italy

ARTICLE INFO

Keywords:
Pre-chamber combustion
Gasoline engine
Lean combustion
Turbulent jet ignition
Computational fluid dynamics

ABSTRACT

Pre-chamber (PC) ignition systems, enabling Turbulent Jet Ignition (TJI) combustion, represent a promising technology to extend the lean limit of Spark Ignition Internal Combustion Engines. Indeed, the higher ignition energy provided by the turbulent jets contributes to the limitation of combustion duration and variability even in diluted conditions. However, a detailed analysis of the combustion process is needed to maximize the performance of the system. More specifically, the interaction between the chemical and the turbulent scales are key factors in assessing the probabilities of main chamber (MC) ignition, determining the ignition pattern, and characterizing the combustion process. For this reason, the development of reliable numerical models is a crucial factor to pave the way toward a deeper understanding of details concerning TJI combustion. In the present work, a 3D-CFD numerical model was validated against experimental data at 4000 rpm, in stoichiometric and lean (i.e., $\lambda = 1.2$) conditions in a single-cylinder gasoline engine equipped with a passive pre-chamber. In both operations, the evolution of the turbulent combustion regimes over the whole combustion process was investigated, highlighting analogies and differences between the selected operative conditions. Additionally, a methodology to characterize the MC ignition and combustion process, able to describe the different phases of the interaction between PC and MC, and assess the thermal, turbulent, and chemical effects of the turbulent jets is presented.

1. Introduction

Nowadays, 99.8% of the transport sector is powered by internal combustion engines (ICEs) [1]. At a global level, road transport accounts for about one-fifth of the overall carbon dioxide emissions [2], which are known to be the largest contribution to global warming [3]. Intending to reach climate neutrality by 2050, in June 2022, the European Commission approved the 'Fit for 55′ climate package [4], which sets zero CO_2 emissions for new cars sold by 2035. To this purpose, many technologies, including battery electric vehicles (BEVs), fuel cell electric vehicles (FCEVs), and hydrogen-fuelled ICEs [5,6], are currently under development. However, the rapid spread of these alternative powertrains is heavily hindered by technical and socio-economical barriers [7,8]. For this reason, the ICE is expected to play a predominant role over

Abbreviations: AMR, adaptive mesh refinement; AFR, air-to-fuel ratio; aTDCf, after top dead centre firing; BEV, battery electric vehicle; CAD, crank angle degree; CCV, cycle-to-cycle variability; CFD, computational fluid dynaimcs; CH_2O, formaldehyde; CJE, cold jet ejection; CPOA, cylinder pressure only analysis; *Da*, Damkholer number; DI, direct injection; ECFM, extended coherent flamelet model; EGR, exhaust gas recirculation; HJE, hot jet ejection; HR, heat release; HRR, heat release rate; ICE, internal combustion engine; IMEP, indicated mean effective pressure; LES, large eddies simulation; MC, main chamber; MFB, mass fraction burned; MON, motored octane number; NA, naturally aspirated; OH, hydroxide; PC, pre-chamber; PFI, port fuel injection; RANS, Reynolds-averaged Navier–Stokes; RON, research octane number; RGF, residual gas fraction; SI, spark ignition; SoC, start of combustion; ST, spark timing; S_L, laminar flame speed; TJI, turbulent jet ignition; TRF, toluene reference fuel; TKE, turbulent kinetic energy; WOT, wide open throttle; WP, working point; WSR, well stirred reaction; δ_L, laminar flame thickness; ϕ, equivalence ratio.

* Corresponding author.
E-mail address: andrea.piano@polito.it (A. Piano).

https://doi.org/10.1016/j.treng.2023.100200
Received 15 May 2023; Received in revised form 27 July 2023; Accepted 3 August 2023
Available online 4 August 2023

the next years [9] and therefore, current research is focusing on key technologies for further improving engine thermal efficiency and reducing emissions [10].

In this framework, lean combustion represents a promising solution for increasing the thermal efficiency of spark ignition (SI) internal combustion engines. This is due to the lowering of the combustion temperature, which leads to a reduction of heat losses through cylinder walls, and the increase of the ratio of specific heats. As the air-to-fuel ratio (AFR) increases, a larger amount of air is inducted into the cylinder, decreasing pumping losses generated by throttling [11,12]. Nonetheless, these positive effects are partially offset by a lengthening of the combustion duration which reduces the ideal thermodynamic efficiency. Moreover, the unstable flame kernel obtained in diluted conditions increases the cycle-to-cycle variability thus reducing the high-efficiency operative range.

Pre-chamber (PC) ignition systems, also known as Turbulent Jet Ignition (TJI), have shown great capabilities in increasing ignition energy, reducing combustion duration, and increasing combustion stability [13–15]. They are made up of a PC connected to the main chamber (MC) through a set of orifices. Combustion is triggered by a spark discharge in the PC, and when PC pressure overcomes that of MC, hot, highly active, and turbulent jets develop in the MC acting as ignition source. Therefore, the local (punctual) ignition mechanism of conventional SI engines is replaced by a distributed (surface) mechanism that makes it possible to extend the lean limit toward higher AFRs. Pre-chamber ignition systems can be classified as active (un-scavenged) and passive (scavenged). In the active pre-chamber configuration, there is a double fuel fed: the injection is performed in the pre-chamber and the fuel is admitted in the cylinder either through direct injection (DI) or Port Fuel Injection (PFI). On the contrary, in the passive pre-chamber configuration, the fuel is pushed inside the PC mainly during the last phase compression stroke as a result of the scavenging process which is driven by the pressure difference that is established between the two combustion chambers. Therefore, the AFR is bounded by the amount of fuel admitted in the main chamber. In the active configuration, the PC fuel injection promotes the scavenging reducing the residual gas concentration [16] and allows the combustion of a PC stoichiometric mixture which was shown to improve the ignition performances and the burn rate achieved in the main chamber thanks to the higher chemical reactivity of the jets [17,18]. These factors allow the extension of the lean limit toward higher enleanment levels. Despite the several advantages related to the adoption of an active pre-chamber, the passive pre-chamber system is particularly promising for automotive applications since its packaging and installation require a small volume, and the limited number of components lowers the cost [19,20].

Especially for passive pre-chamber configurations, the definition of its main geometrical features is of paramount importance for increasing thermal efficiency and ensuring a stable engine operation under a wide range of operating conditions. Indeed, pre-chamber combustion is mainly governed by its local conditions, in terms of residual gas fraction (RGF) and turbulent kinetic energy (TKE), which result from the scavenging and filling processes. They begin during the intake process, but most of them take place during the compression stroke, just before the spark event [21–23], and are controlled by the geometry of the pre-chamber. Therefore, the time available for the fresh gases to reach the spark plug region and replace residual burnt gases, thus ensuring fast flame propagation is limited and strongly related to PC geometrical characteristics.

Nonetheless, the speed at which the flame front sweeps the pre-chamber volume is closely tied to the turbulence intensity and its spatial distribution. PC turbulent flow field is generated during the scavenging process as a result of the interaction between the high-speed jets that enters through the orifice when MC pressure exceeds that in the PC [24]. This mechanism leads to the stratification of the turbulent flow field and causes the average level of turbulence to increase significantly. All things considered, the interaction between chemical and turbulent quantities is a crucial element to determine pre-chamber combustion characteristics.

The ignition of the main chamber charge relies on thermal, chemical, and turbulent effects [25]. The chemical contribution refers to the composition of the hot jets, which contain highly chemically reactive species (O, H, and OH) resulting from PC combustion. Additionally, the large pressure difference established during PC combustion between the two combustion chambers generates high-speed jets which result in long penetration distances and high air entrainment rates. This helps in spreading active radicals over a wider region of the main combustion chamber that could potentially trigger combustion. Finally, the strong velocity gradients induced by the jet ejection increase turbulence intensity promoting higher turbulent flame speeds in the combustion phases following the ignition of the mixture. Nonetheless, if turbulence intensity exceeds a certain threshold, the local breaking of chemical reactions induced by the smallest turbulent eddies and the cooling effect caused by the rapid mixing between the jets and the fresh charge may cause the flame to extinguish.

For these reasons, the interaction between the chemical and the turbulent scales has a fundamental role in assessing the probabilities of MC ignition, determining the ignition pattern, and characterizing the combustion process. Mastorakos et al. [26] experimentally investigated the TJI mechanism at atmospheric pressure in an optically accessible PC fuelled with ethylene and methane. Experimental results made it possible to describe in detail the passage of the flame through the orifice and the structure of the jet exiting from the PC for different nozzle diameters. Biswas et al. [27] identified two ignition mechanisms namely jet ignition and flame ignition for premixed mixtures of CH_4/air and H_2/air. In the first mechanism, the PC flame is quenched when passing through the nozzles and MC combustion is triggered by the hot combustion products delivered by the PC. As the orifice diameter increases, a jet of wrinkled turbulent flames containing incomplete combustion products can emerge in the MC. This ignition mechanism is called flame ignition and reduces the ignition delay if compared to the jet ignition mechanism. Additionally, it was defined a critical Damköhler number to distinguish ignition cases from non-ignition cases.

Even though experimental campaigns can provide useful details on the complex mechanisms that govern PC ignition systems, the measurement of high-quality data in an actual engine process is challenging because of the small dimensions of the system and its tight integration into the cylinder head. In this context, 3D-CFD numerical simulations based on Reynolds Averaged Navier–Stokes (RANS) approach can add useful insights, by gathering data that cannot be experimentally studied, significantly reducing the lead time and the development costs. Novella et al. [28] performed a numerical study to analyse the performance of a passive pre-chamber gasoline ignition system under three engine relevant operating conditions, identifying the most critical working points. Ge et al. [29] combined 3D CFD simulations with genetic algorithm and machine learning to optimize the pre-chamber design for a spark ignition gasoline engine. In the literature exists several studies that describe

the interaction between turbulence and chemistry based on results obtained from 3D-CFD numerical analysis [30,23,31]. Usually, these analyses are performed starting from the outcomes of combustion models that rely on the flamelet assumption, such as the G-equation model [30, 31], Extended Coherent Flamelet Model (ECFM) [23], while limited results based the Well Stirred Reaction (WSR) assumption are available in the literature. Even though combustion models based on a WSR approach do not intrinsically consider the turbulence chemistry interaction (TCI), they may allow increasing the predictive capabilities of the numerical model, by drastically reducing the need of calibrating the combustion model. In such a context, the goal of this research is first to assess the capabilities of a WSR combustion model to replicate the experimental measurements. Afterward, a methodology for characterizing turbulence and chemistry adopting numerical simulations that take exploit a combustion model based on detailed chemistry is proposed.

Experimental tests were carried out at CNR STEMS laboratories in Naples, while numerical simulations were performed at the HPC@POLITO, the High-Performance Computing centre of the Politecnico di Torino.

The paper is organized as follows: first, the numerical setup of the 3D-CFD model is presented and the validation of the numerical model against experimental data is shown. Then, the paper will focus on the analysis of the interaction between turbulence and chemistry-related quantities throughout the entire combustion process, highlighting analogies and differences between stoichiometric and lean operating conditions. Finally, for the same working points, a methodology for assessing the MC ignition mechanism and tracking the key parameters of MC combustion will be presented.

2. Case study

2.1. Engine specifications

Experimental tests to calibrate the numerical model were carried out on a naturally aspirated (NA) gasoline four-stroke SI single-cylinder metal engine, whose main features are reported in Table 1.

The engine architecture is the same as used in [32]. The original SI engine was equipped with a pent-roof, four-valve head, with a centrally-mounted spark plug. Fuel was admitted in the cylinder through a PFI system, with an injection pressure of 3 bar, located in the intake manifold to ensure the homogeneity of the mixture. Due to the pre-chamber volume, which raises the clearance volume (V_C), the compression ratio was decreased to 10.5 in the TJI configuration, starting from 11.5 in the conventional SI engine. More details and specifications are reported in [33].

Table 1
Main specifications of the SI single-cylinder engine.

Displacement	cm^3	250
Bore	mm	72
Stroke	mm	60
Compression Ratio	–	11.5 (SI) 10.5 (TJI)
Max Power	kW	16 @ 8000 rpm
Max Torque	Nm	20 @ 5500 rpm

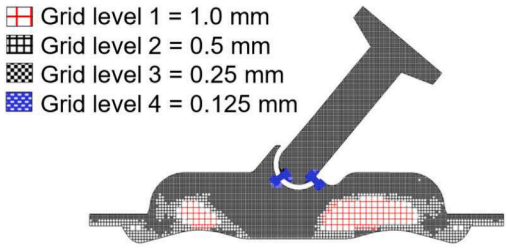

Fig. 1. Cross section of the combustion system assembly with the piston at the TDC.

Table 2
Pre-chamber specifications.

Volume	cm^3	2.2
V_{PC}/V_C	%	7.2
Number of nozzles	–	4
Nozzle diameter	mm	1
A_{nozzle}/V_{PC}	cm^{-1}	0.017

2.2. Pre-chamber specifications

Fig. 1 displays the geometrical features of the combustion system by means of a cross-sectional plane passing through the spark plug axis, with the piston at TDC.

The pre-chamber, properly designed to fit within the original spark plug seat, has a volume of 2.2 cm^3, which corresponds to 7.2% of the clearance volume, as shown in Table 2. This value is considerably higher if compared to the most common literature values (2.0%−3.5%) [34, 35]. This leads to a significant compression ratio reduction to such an extent that it could partially mitigate the beneficial effect of a TJI operation. Nonetheless, being the aim of the work the definition of a numerical methodology for characterizing TJI combustion and describing the phenomena that govern the ignition process, rather than the maximization of the system performances, the large CR reduction has been considered out of scope.

An additional element, positioned above the PC, contains the injector and the spark plug housings making it possible to operate the TJI system both in active (not used in the present work) and passive modes. A large length-to-diameter ratio is needed to guarantee enough space for the injector and spark plug housings avoiding any modification of the cylinder head and the intake ports. It is worth pointing out that this aspect, together with the passive operational mode and the small ratio between the total nozzle area and the PC volume (A_{nozzle}/V_{PC}), which usually ranges between 0.025 cm^{-1} and 0.045 cm^{-1} [36], heavily hinders pre-chamber scavenging and filling processes and the development of suitable conditions for mixture ignition and combustion near the spark plug, thus leaving plenty of room for the PC geometrical optimization.

2.3. Test matrix

Experiments were performed on the Wide Open Throttle (WOT) curve in stoichiometric and lean conditions at 2000, 3000, and 4000 rpm, whereas only the stoichiometric condition was tested at 5000 rpm due to the combustion instability at high engine velocity in diluted conditions. To obtain a statistically representative sample, pressure traces of 400 consecutive working cycles were recorded for each of the tested working points. The AFR was measured through a lambda sensor installed in the engine exhaust pipe. While in [32], the analysis was

Table 3
Operating conditions considered for the numerical analysis.

4000 rpm	IMEP bar	COV_{IMEP} %	ST CAD aTDCf
WP #1 Lambda 1.0	9.71	0.785	−25
WP #2 Lambda 1.2	8.73	2.32	−69

conducted in the two working points at 3000 rpm, in the present work, the numerical analysis was carried out in two working points at 4000 rpm in stoichiometric ($\lambda = 1.0$) and lean conditions ($\lambda = 1.2$), as reported in Table 3 together with the spark timing (ST), the Indicated Mean Effective Pressure (IMEP), and its coefficient of variation (COV_{IMEP}).

3. Simulations

3.1. Setup

Simulations were carried out in the commercial software CONVERGE CFD v3.0. A proprietary cut-cell Cartesian grid generation method was used for generating mesh at runtime. The base grid size was set equal to 2 mm, and through a series of local mesh refinements, a minimum cell size of 0.125 mm was reached inside the PC holes (Fig. 1). Moreover, the Adaptive Mesh Refinement (AMR) algorithm was employed to increase the grid refinement level only in the regions characterized by high velocities and large temperature gradients (e.g. flame front), without excessively slowing the simulation with a uniformly refined grid. This approach led to a total number of cells in the computational domain between 700.000 during the compression stroke and 3 million at the end of the combustion phase. Time-varying pressure and temperature profiles, evaluated through the 1D model previously validated against experimental data in GT-SUITE, were applied as inflow and outflow boundary conditions. The same 1D-CFD model was used to define the chemical composition of the gases entering the computational domain. Fuel injected by the PFI system was considered entirely vaporized and perfectly mixed with air in the intake port. Turbulence modelling is particularly important for correctly predicting turbulence evolution during the entire engine cycle since it influences both PC flow pattern and MC jet penetration and ignition. A Reynolds Averaged Navier–Stokes approach was used, coupled with the $k-\varepsilon$ with renormalization group (RNG) turbulence model [37], widely employed for ICE applications, capable of taking into account several key physical phenomena related to ICE combustion, such as compressibility and rapid strain effects. Additionally, this turbulence model was adopted by the authors in previous activities [38,39], showing good capabilities in replicating the experimental data. Near-wall thermal and kinetic boundary layers were described through the law of the walls functions, and heat transfer was modelled through the Han and Reitz functions [40]. For what concerns combustion simulation, the SAGE detailed chemical solver [41,42] was adopted. It relies on the Well Stirred Reactor (WSR) hypothesis. This choice is based on several arguments. First, the detailed chemical model demonstrated to account for multiple and distributed ignition points inside the MC (premixed and partially premixed combustion regimes). In addition, in the operating conditions characteristic of a TJI operation (lean conditions and highly turbulent flow fields), assumptions on which flamelets-based models (e.g. G-equation and ECFM) are based may no longer be valid [43]. Although the adoption of the SAGE combustion model could be considered questionable, since it does not take into account the interaction between turbulence and chemistry, it has been selected since it allows the tracking of the chemical species throughout combustion progress, for instance needed for the evaluation of auto-ignition as reported in [38]. In addition, in light of the wide area of the combustion regimes crossed by the TJI combustion, which goes from Da

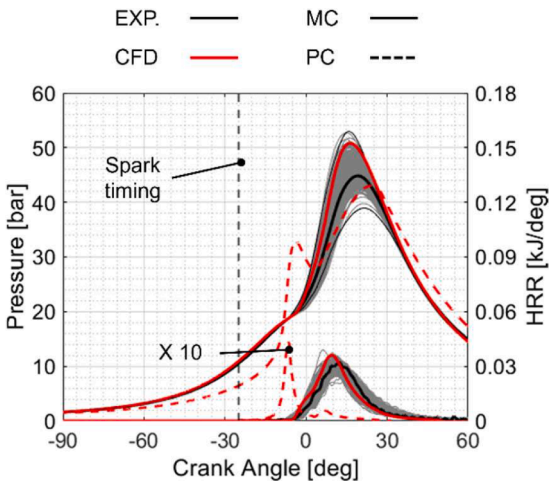

Fig. 2. Working Point #1 (Stoichiometric): comparison between experimental median (black), 400 consecutive working cycles (grey) pressure and heat release rate, and 3D-CFD model results (red). Main chamber (solid line) and pre-chamber (dashed line).

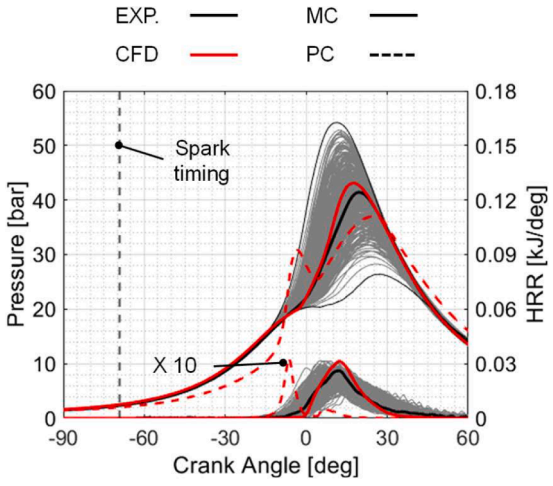

Fig. 3. Working Point #2 (Lean): comparison between experimental median (black), 400 consecutive working cycles (grey) pressure and heat release rate, and 3D-CFD model results (red). Main chamber (solid line) and pre-chamber (dashed line).

$<< 1$ during the jet ignition process to $Da > 1$ during the flame propagation combustion, it does not appear to exist a unique combustion model suitable for all the combustion phases [44]. Furthermore, a combustion model based on the WSR assumption has been successfully adopted in several research studies available in the literature [39,43,45], thus corroborating its selection in the present work. Finally, the adoption of a sufficiently refined mesh leads to well-resolved flow field, decreasing the need for a turbulence chemistry interaction model to capture the enhanced diffusion by turbulence [46,47]. This combustion model requires the definition of a fuel surrogate and the choice of a combustion mechanism. The Toluene Reference Fuel (TRF) proposed in [48] and made up of 71,36% toluene (C_7H_8), 6,60% isooctane (C_8H_{18}), 22,04% n-heptane (C_7H_{16}) was adopted to approximate the main characteristics, in terms of RON and MON, of the gasoline used for the experimental tests. The combustion mechanism proposed in [49], which features 165 species and 839 reactions, was adopted to replicate the combustion process. Ignition was modelled through an L-shape energy shape to model the breakdown and the arc and glow phases. For this purpose, two identical spherical shape sources with an equivalent

energy content of 20 mJ, but a duration ratio of one to ten were positioned between the spark plug electrodes. For additional details regarding the numerical setup refer to [32].

3.2. Results

In Fig. 2 and Fig. 3 the comparison between experimental and numerical results, in terms of MC and PC pressure and heat release rate (HRR) is shown. For each of the selected working conditions, the 400 consecutive cycles are depicted in grey, while the black line is representative of the median cycle identified by sorting the 400 consecutive cycles in ascending order based on the peak pressure value. To ensure consistency between experimental data and the results obtained from the numerical model, all the HRR curves were obtained by processing the pressure traces through a 1D Cylinder Pressure Only Analysis (CPOA) model in GT-SUITE. Numerical results referred to the prechamber are displayed by the dashed line, whereas main chamber results are shown by the solid line. It's worth pointing out that PC pressure measurements are not available. Nonetheless, in both the working points analysed, a generally good agreement between experimental data and simulation results is obtained. In the stoichiometric condition (WP #1), the start of MC combustion is correctly captured by the model. Then, the model slightly overpredicts the flame propagation speed and a higher HRR peak is reached, leading to a maximum pressure value higher than the median cycle. However, both the HRR and the pressure curves remain within the combustion variability range resulting from the experimental campaign. The higher degree of mixture dilution and the slower combustion rate in the lean working point (WP #2) requires advancing the spark timing by 44 Crank Angle Degrees (CAD) in comparison with the stoichiometric working condition. The reduction of the available time for PC scavenging and the mixture enleanment make the ignition process even more unstable, thus increasing the CCV, as reported in Table 3. As far as the predictive capabilities are concerned, the numerical model shows a good agreement also at $\lambda = 1.2$ operation, even if a small delay in the predicted MC start of combustion (SoC) can be noticed.

4. Turbulence-chemistry analysis

Pre-mixed combustion is a phenomenon characterized by a complex interaction between chemical reactions and the turbulent flow field, which corrugating the flame front increases the flame surface area, promoting higher burning velocity. In a conventional SI engine, the turbulent flow field is produced by means of the high shear flows generated during the intake process and partially conserved during the compression stroke thanks to the conversion of the well-organized in-cylinder motion patterns into turbulent kinetic energy. Instead, in PC combustion systems, the TKE generated in the main chamber during the intake process represents a small portion, the less energetic one, of the overall turbulences observed in the main combustion chamber during the combustion process. Indeed, as shown in [50], the most intense turbulence is produced by the turbulent jets exiting the PC. Furthermore, compared to traditional SI engines, the turbulent flow field is highly inhomogeneous, has large spatial gradients at the jet boundaries, and exhibits a rapid temporal evolution. In addition, turbulent fluctuations of the velocity field near the spark plug are the result of the high-speed jet-to-jet interaction which is produced during the scavenging process due to the nozzles throttling effect.

The interaction between turbulence and chemistry-related quantities plays a fundamental role in determining combustion characteristics amongst which the most crucial for TJI applications are the ignition of the PC charge, the speed of flame propagation in the PC, the MC mixture ignition mechanism, and its burning rate. Therefore, in the following section the turbulent regimes crossed by the flame front throughout the entire combustion process, from the spark timing to the 90% of mass fraction burnt (MFB90) are numerically computed for the two working points displayed in Table 1 and reported on the well-known Borghi–Peters diagram [51,52].

To this purpose, it is useful to define dimensionless characteristic numbers which correlate chemical and turbulent quantities. These allow the identification of different regimes of turbulent flames on the Borghi–Peters diagram. In the present work, the following two dimensionless numbers are used to describe the nature of the turbulent flames:

- Damköhler number (Da) is computed as the ratio between the characteristic integral eddy turnover time (τ_T) and the laminar burning time (τ_L)

$$Da = \frac{\tau_T}{\tau_L} \tag{1}$$

  where:
  - τ_T is the ratio between the integral length scale l_I and the turbulent intensity of the eddies characterized by an integral length scale u'
  - τ_L is the residence time in a laminar flame computed as the ratio between the laminar flame thickness δ_L and the laminar flame speed S_L
- First Karlovitz number (Ka) is computed as the ratio between the chemical time scale τ_L and the eddy turnover time at the Kolmogorov scale τ_η

$$Ka = \frac{\tau_L}{\tau_\eta} \tag{2}$$

For Ka smaller than one ($Ka < 1$), any turbulent time scale is larger than the chemical time scale. Moreover, the turbulent length scales associated with the smallest eddies (i.e. Kolmogorov scales) are larger than the flame thickness. Therefore, turbulent fluctuations do not substantially perturb the flame structure. However, there is a kinematic interaction between the laminar flame front and the turbulent flow field that causes the corrugation of the flame front. As the turbulence intensity increases ($Ka > 1$ and $Da > 1$), the smallest eddies are able to penetrate and modify the structure of the flame. Therefore, the flame front becomes thicker and more corrugated. For $Da < 1$, the scalar mixing of the reaction zone fluid with the unburned mixture is further intensified. In such conditions, the integral eddy turnover time is smaller than the laminar burning time. Therefore, combustion is mainly limited by chemistry. Finally, for $Ka > 100$, turbulence intensity is so high that the Kolmogorov eddies can penetrate the inner layer, broken down chemical oxidation reactions thus extinguishing the flame [53].

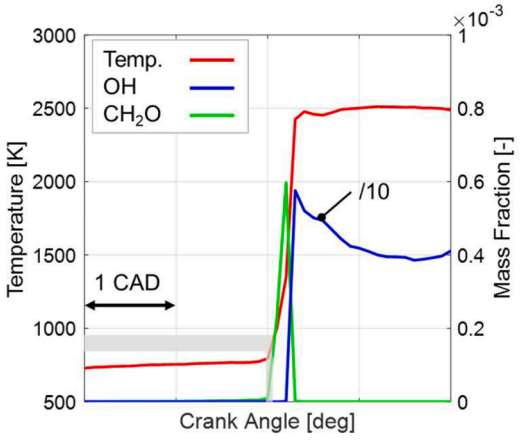

Fig. 4. Temperature, CH_2O, and OH mass fraction evolution concurrently with the flame front passage.

4.1. Methodology

Starting from the results of the validated numerical simulations, the first step consisted of the identification of the flame front position within the time interval from spark timing to 90% of the mass fraction burnt. Indeed, the SAGE Detailed Chemical Kinetics Solver used for combustion simulation does not automatically track the position of the flame front through specific variables, as it happens for combustion models based on the flamelet assumption. Since formaldehyde (CH_2O) is a radical representative of low-temperature pre-flame reactions that take place in the unburned gases in gasoline-fuelled engines, it has been selected to track the position of the flame front. Indeed this chemical species is present in high concentrations in the cool flame while it is completely consumed when reached by the hot flame front. Therefore, thanks to this peculiarity it can be used to accurately identify the location of the flame front [38]. Fig. 4 shows the evolution of temperature, formaldehyde, and OH mass fractions evaluated in a fixed point within the main chamber. The fast temperature and OH concentration increase are indicative of the passage of the flame front. Before this, the progress of pre-flame reactions is highlighted by the growth of the concentration of formaldehyde. In particular, it can be noticed that the rate of increase of formaldehyde in the unburned gases was relatively slow where the temperature was lower than 850 K. For higher temperatures, its concentration rapidly increases, before disappearing consumed by the advancing flame front. In correspondence with the abrupt rise in the slope of the CH_2O mass fraction, an upper-temperature threshold of 950 K was identified. Finally, the portion of the unburned gases that is going to be consumed by the flame front was then marked using the temperature range that was so determined.

The second phase of the proposed methodology concerns the evaluation of the laminar flame speed (S_L) and laminar flame thickness (δ_L), since these values are not intrinsically provided as outputs of the 3D-CFD simulation. To this purpose, the 1D laminar premixed flame chemistry tool of Converge 3.0 was employed. S_L and δ_L are computed in a mono-dimensional domain considering a planar flame propagating in a perfectly homogeneous mixture. A wide test matrix, reported in Table 4, was defined with the aim of covering the entire range of pressure, temperature, residual concentration, and equivalence ratio encountered by the flame during the combustion process, both in PC and MC.

Turbulent quantities are provided by the 3D-CFD simulation in which turbulent length scale (l_I) and turbulent velocity (u') are computed from the turbulent kinetic energy (k), the turbulent dissipation (ε), and the turbulent viscosity coefficient (C_μ), under the assumption that each cell is sufficiently small to ensure the homogeneity and isotropy of the turbulent flow field.

$$l_I = C_\mu^{0.75} \frac{k^{\frac{3}{2}}}{\varepsilon} \tag{3}$$

$$u' = \sqrt{\frac{2}{3}k} \tag{4}$$

Finally, the length scale ratio u'/S_L and the velocity scale ratio l_I/δ_L were computed in all the cells with a temperature between the previously defined thresholds and averaged on a mass basis.

Table 4
Test matrix for which laminar flame thickness δ_L and the laminar flame speed S_L were computed.

	Min	Max	Step
Pressure [bar]	5	60	5
Temperature [K]	600	1300	50
Φ [-]	0.4	2.0	0.2
EGR [-]	0.0	0.9	0.3

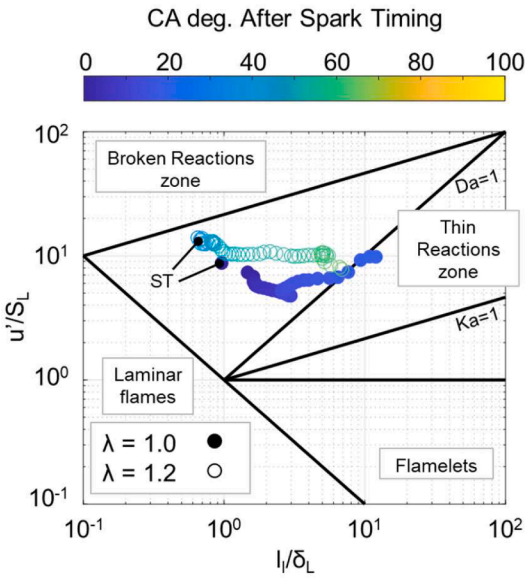

Fig. 5. Evolution of the turbulent regimes during pre-chamber combustion from spark timing to the ejection of the hot gases in the main chamber (step 0.5 CAD). Stoichiometric conditions (λ = 1.0) solid dots, Lean conditions (λ = 1.2) empty dots.

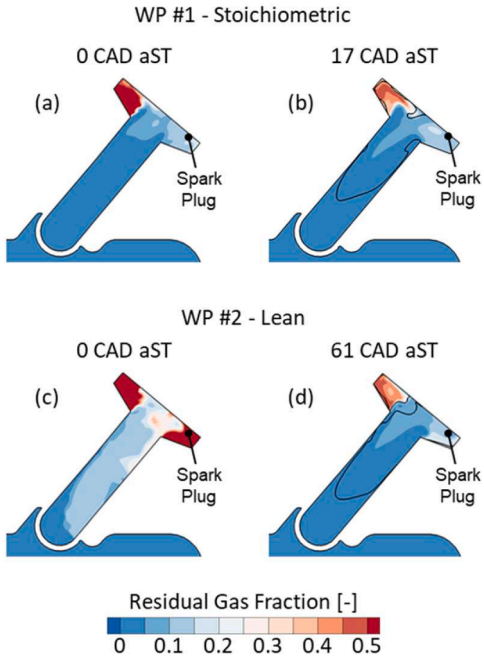

Fig. 6. Pre-chamber Residual Gas Fraction concentration for stoichiometric (top) and lean (bottom) mixture conditions. The black line represents the position of the flame front.

4.2. Pre-chamber turbulent combustion regimes

Fig. 5 shows the evolution of the turbulent regimes in PC for the stoichiometric (WP #1) and lean (WP #2) operating conditions, filled and empty circles respectively. In stoichiometric conditions, the entire PC combustion evolves in the thin reaction zone due to the high turbulence level generated by the interaction between the high-speed jets entering the PC during the last phase of the compression stroke. As shown in Fig. 6a, in WP #1, at spark timing, PC residuals are stratified, with a higher concentration in the upper part of the pre-chamber. The

higher residuals concentration leads to a reduction of the S_L and an increase of the δ_L, which force combustion to start in the upper-left part of the thin reaction zone. As combustion proceeds, the increase of PC pressure reduces the gap with MC pressure, decreasing the speed of the incoming jets and thus the turbulence intensity. For this reason, the velocity scale ratio decreases at first. Then, as the flame approaches the bottom section of the PC (Fig. 6b), the u' reduction is balanced by the increase of the S_L due to the significant reduction of residual concentration on the flame front, and the velocity scale ratio increases again. In the meantime, l_I remains almost constant and uniform on the flame front surface. As observed for S_L, δ_L reduces too as the flame proceeds toward the lower part of the PC thanks to the decrease of residual gases. Thus, the length scale ratio increases toward larger values to the point that the turbulent regime crosses the $Da = 1$ line just before the appearance of the hot jets in the MC. When a leaner mixture is considered (WP #2), the time needed by the flame front to reach the PC nozzles, is considerably higher than in stoichiometric conditions (WP #1). Indeed, while in WP #1 PC combustion lasts 19.5 CAD, in WP #2 the flame sweeps the PC volume in 60 CAD. This is because when the engine is operated with excess air, combustion starts in a less favourable region. Indeed, the large spark advance partially hinders the scavenging of the pre-chamber to such an extent that at the spark time, more than 50% of the mixture is made up of residuals near the spark plug (i.e. 53.1%), as reported in Fig. 6c. The high residual concentration and the relatively low turbulence level constrain the flame in the upper part of the PC for more than 40 CAD. Moreover, the low S_L and the high δ_L in diluted conditions move the turbulent combustion regimes nearer to the broken reactions zone compared with the stoichiometric operation. When the flame reaches the cylindrical portion of the pre-chamber (Fig. 6d), which is characterized by stronger turbulence, its evolution follows the same path observed for the stoichiometric working point. Nonetheless, the higher δ_L and the lower S_L in diluted conditions move the curve upward. From the turbulence-chemistry analysis, it is clear that the operation of passive pre-chamber systems with lean mixtures is particularly challenging at high engine speeds due to the combination of the advanced spark time required to correctly phase MC combustion and the low laminar flame speed, which could jeopardize combustion stability. For this reason, the optimization of the pre-chamber geometry plays a key role in reducing the CCV and extending the lean limit.

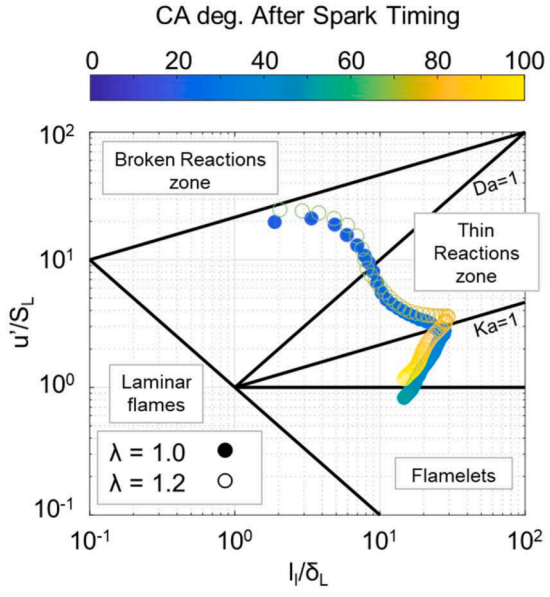

Fig. 7. Evolution of the turbulent regimes during main chamber combustion from the start of main chamber combustion to MFB90 (step 0.5 CAD). Stoichiometric conditions (λ = 1.0) solid dots, Lean conditions (λ = 1.2) empty dots.

4.3. Main chamber turbulent combustion regimes

Fig. 7 displays the evolution of the turbulent regimes associated with main chamber combustion in stoichiometric (WP #1) and lean (WP #2) conditions. Compared to pre-chamber combustion, main chamber combustion spans a wider area of the Borghi–Peters diagram, moving from the border of the broken reactions zone to the flamelets region, passing through the thin reaction zone. In TJI systems, the interaction between turbulence, chemistry, and thermal effects during the ejection of the pre-chamber burnt gases is a crucial factor since it determines the ignition mechanism (i.e., flame ignition or jet ignition) and the probabilities of ignition. Indeed, when the hot gases are ejected in the MC, their high turbulent velocity increases the turbulence intensity experienced by the flame front, moving the turbulent regimes toward the broken reaction zone. If the turbulent regimes fall in the broken reactions zone, the extremely rapid mixing between the hot jet and the cold MC mixture induced by the strong turbulent velocities increases the probability of non-ignition [27]. In the present study, the first part of the main chamber combustion is near the $Ka_\delta = 1$ for both the operating conditions without exceeding it. Here, the Kolmogorov eddies can penetrate the preheat zone, but they are not sufficiently small to enter the inner layer disrupting the chemical reactions and extinguishing the flame. For this reason, the flame is able to survive and ensure the ignition of the MC mixture. However, in the lean working point (WP #2), the reduction of S_L increases the velocity scale ratio, bringing the turbulent regime closer to the broken reaction zone. Additionally, 3 CAD are approximately needed before the velocity scale ratio starts to decrease significantly, whereas in WP #1 the same velocity scale reduction is observed in 2 CAD. These two factors could explain the longer time observed in WP #2 between the appearance of the hot jet and the start of MC combustion. Then, as the jet intensity decreases, the turbulent speed reduces, and combustion evolves first in the thin reaction zone moving toward the flamelets region. Finally, when the jet-induced turbulences disappear and the flame approaches the boundary of the combustion chamber, combustion moves linearly in the corrugated and wrinkled regions. From a general perspective, a similar trend can be noticed between the two working points considered. Nonetheless, as the mixture becomes leaner, the reduction of S_L and the increase of δ_L shift the turbulent regimes toward the upper part of the diagram. Overall, the comparable evolution of the turbulent regimes during MC combustion well reflects the similar duration of the combustion observed in stoichiometric and lean conditions, emphasizing once again the potentialities of this analysis in predicting combustion behaviour. From a numerical perspective, the wide area of the Borghi–Peters diagram that is swept during the combustion process indicates the need for a hybrid combustion model. Indeed, for simulating PC combustion and MC ignition, a combustion model based on the WSR assumption would be preferable, whereas a flamelet-based model would be more suitable for describing MC combustion.

4.4. Main chamber ignition and local Damköhler number

The characterization of the connection between turbulence and chemistry that has been presented so far is a useful tool for globally characterizing main chamber combustion process. Nonetheless, as the hot jets move away from the outlet section of the PC nozzles, the impact with the MC fresh mixture and the impingement with the piston top distinguish the turbulence intensity on the boundary of the jet. This causes the formation of some regions in which the role of chemistry is predominant on that of turbulence and vice versa. Thus, in order to understand how jets ignite the MC mixture and the combustion propagations from a spatial perspective, it can be helpful the evaluation of the Damköhler number on the surface that marks the flame front. Fig. 8 displays the Damköhler number computed on the same isotemperature surface used to mark the position of the flame front as reported in the previous paragraph. In the figure, six consecutive snapshots are depicted

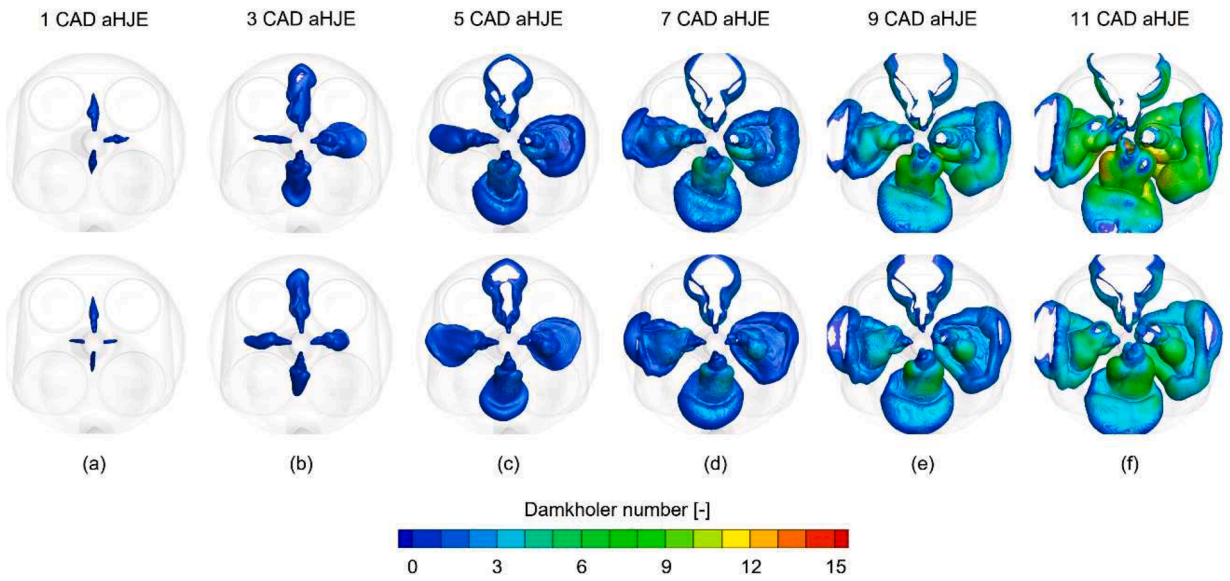

Fig. 8. Damköhler number on the flame front surface at stoichiometric (top) and lean (bottom) conditions using local temperature to track the position of the flame front. Five snapshots are depicted (with steps equal to 1 CAD) at a constant interval from the ejection of the hot jets.

starting from 1.0 CAD (step 2 CAD) after the ejection of the hot jets both at stoichiometric (WP #1, top) and lean (WP #2, top) conditions. In agreement with the results shown in Section 4.3, in both operating conditions, the global Damköhler number remains well below the unitary value for approximately 3 CAD after the start of the Hot Jets Ejection (HJE) as confirmed by Fig. 8a and Fig. 8b. This is due to the extremely strong turbulence intensity observed within this temporal frame. This indicates that the turbulent time scale is lower than the chemical one by more than one order of magnitude. Therefore, turbulent fluctuations instantaneously mix products and reagents, and combustion is limited by the speed of the chemical reactions. Then, as the jets travel across the main chamber, the air that is entrained radially with respect

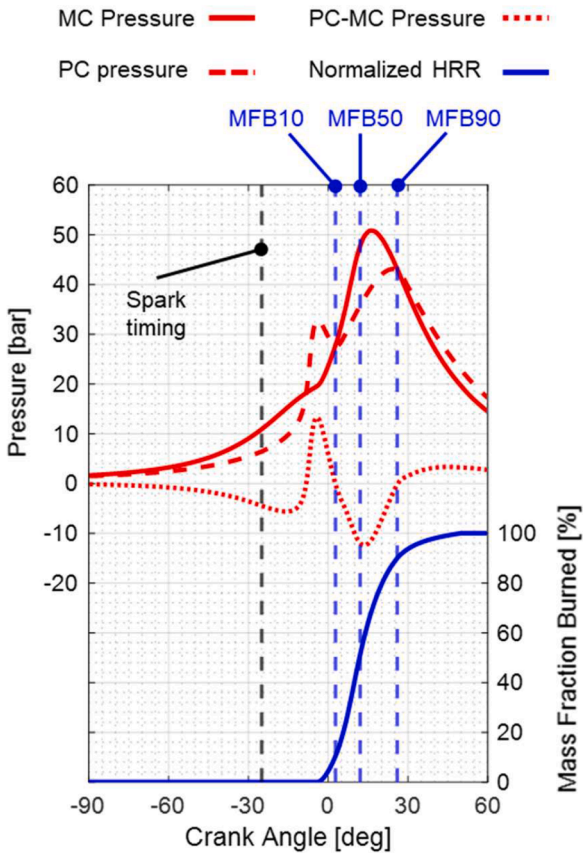

Fig. 9. Evolution of main and pre-chamber pressure and pressure difference between pre-chamber and main chamber, and main chamber heat release in the stoichiometric ($\lambda = 1.0$) working point (WP #1).

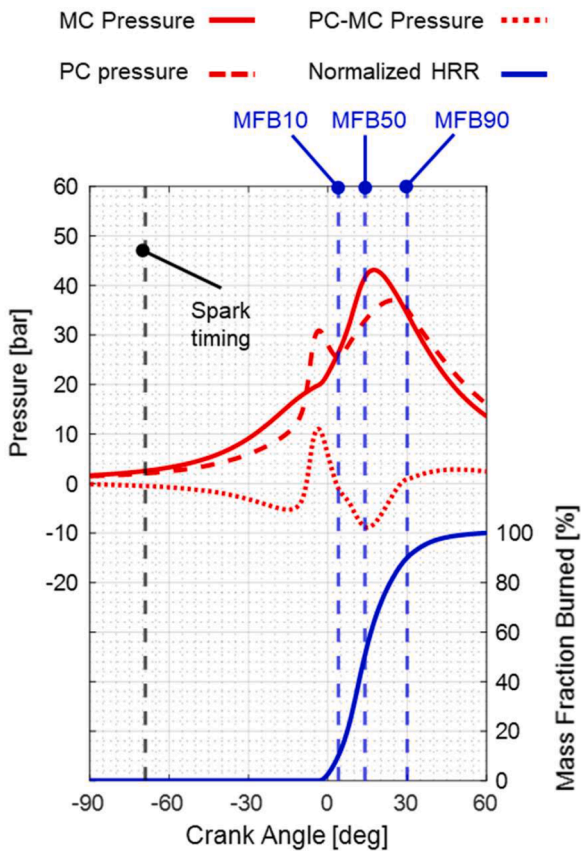

Fig. 10. Evolution of main and pre-chamber pressure and pressure difference between pre-chamber and main chamber, and main chamber heat release in the lean ($\lambda = 1.2$) working point (WP #2).

to the axis of the jet, reduces the intensity of the turbulent flow field, thus increasing the Damköhler number. However, it can be also seen that in stoichiometric conditions (WP #1), the higher S_L and the smaller δ_L lead to a faster rise of the Damköhler number. According to the premixed combustion theory, this aspect favors the development of a highly wrinkled flame front that, as confirmed by Fig. 8c and Fig. 8d, propagates faster in stoichiometric conditions (WP #1) than in lean conditions (WP #2). Then, with a delay of 2 CAD (7 and 9 CAD after HJE in WP #1 and WP #2 respectively), when the ejection process is over, the same behaviour is noticed on the portion of the jet that impinges on the piston top. Finally, in accordance with the turbulent combustion regimes plotted on the Borghi–Peters diagram, 11 CAD after the start of the HJE (Fig. 8f) a general reduction of the Damköhler number is observed on the entire surface of the jet. This suggests that unburned gases are consumed by a compact propagative flame front, as it happens in conventional SI engines. Nonetheless, in contrast to the latter, turbulence generated by the jets does not disappear immediately after the end of their ejection, but it takes time to dissipate. This aspect prevents the Damköhler

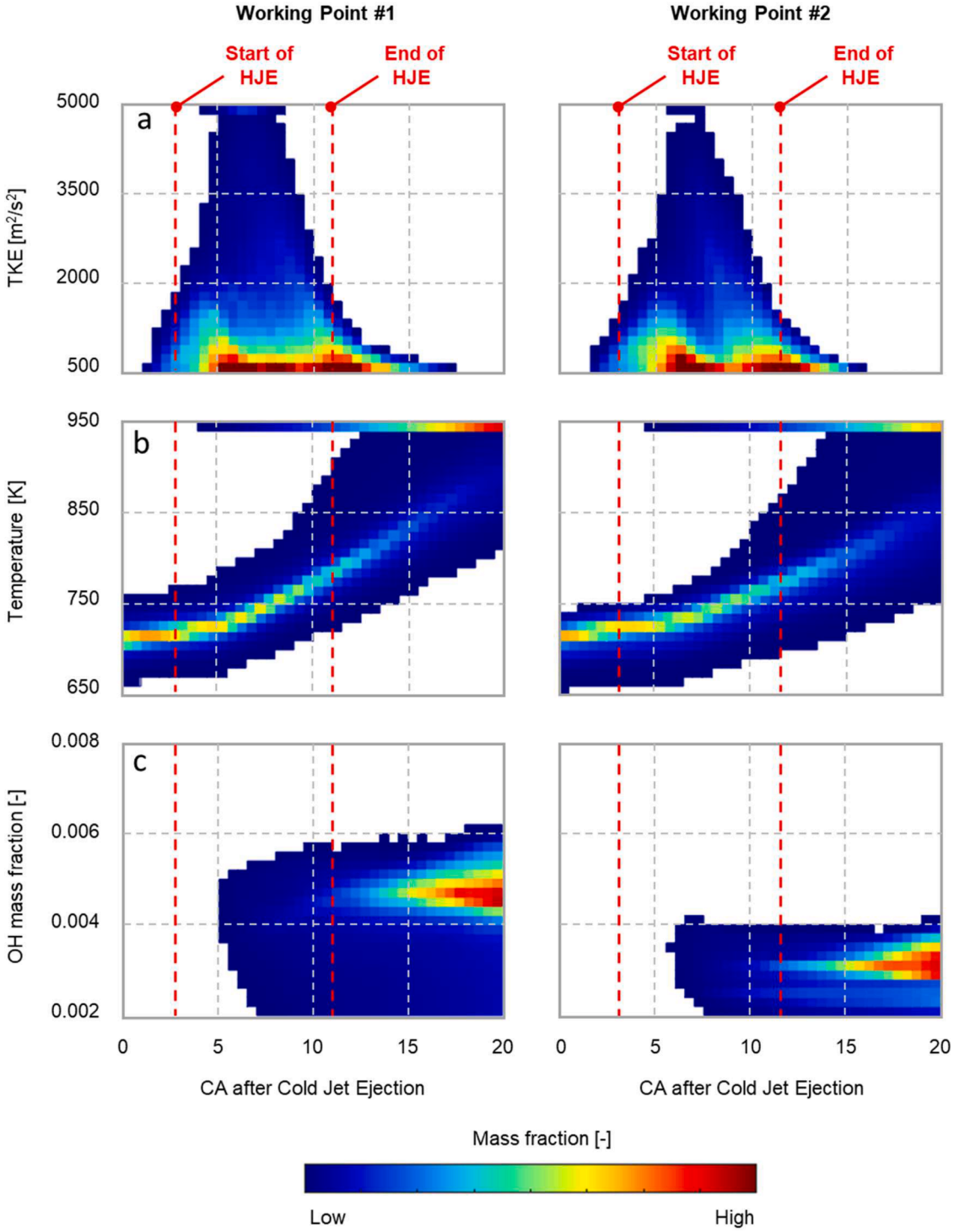

Fig. 11. Turbulent kinetic energy (a), temperature (b), and OH (c) distributions measured in the main chamber after the ejection of the cold turbulent jets. The left column refers to the stoichiometric working condition (WP #1) and the right column to the lean working point (WP #2).

number from rapidly increasing. Indeed, even after the end of the ejection, on average the Damköhler number is smaller than 10. Therefore, the propagating flame front is still corrugated by the turbulences induced by the jets, helping in increasing combustion speed, as expected in PC-equipped engines.

5. Combustion analysis

Figs. 9 and 10 show the pressure evolution inside the main and pre-chamber and their pressure difference together with the main chamber burnt fraction for the two operating conditions reported in Table 3. Due to the throttling effect of the connecting nozzles, pre-chamber pressure is lower than the main chamber pressure during the last phase of the compression stroke. Then, as the flame propagates from the spark plug toward the PC nozzles, the rapid expansion of the hot and low-pressure gases pushes fresh gases through the connecting ducts. In this phase, main chamber combustion has not yet started, as confirmed by the burnt fraction curve, which remains equal to zero for 0.3.2 CAD and 3.8 CAD after the start of the Cold Jets Ejection (CJE) respectively for WP #1 and WP #2. In stoichiometric conditions (WP #1), the larger mass of fuel which filled the pre-chamber during the compression stroke and the stoichiometry of the mixture lead to a more intense PC combustion and a faster heat release (HR). Thus, in this working point, the maximum pressure difference is equal to 13.2 bar whereas in lean conditions, a smaller value equal to 11.0 bar is achieved. The start of main chamber combustion begins at 4.7 CAD and 3.8 CAD before TDCf for WP #1 and WP #2 respectively, with a delay equal to 1 CAD with respect to the appearance of the hot turbulent jets in the main chamber and is sustained by the Hot Jets until MC pressure exceeds that in the pre-chamber. A similar duration of the ejection processes can be noticed for the two working conditions analysed since the lower reactivity of WP #2 is counterbalanced by the lower amount of energy released.

Overall, in stoichiometric conditions (WP #1), combustion duration, computed as the difference between MFB90 and MFB10, is equal to 23 CAD, while combustion lasts 26 CAD in lean conditions (WP #2). This relatively minor difference confirms the goodness of the pre-chamber ignition system in containing combustion duration adopting lean mixtures.

5.1. Main chamber ignition mechanism

As already stated, the ignition process of the main combustion chamber is triggered by the jets that result from the pre-chamber combustion. Several properties of the high-velocity jets contribute to this process. These are the turbulent, thermal, and chemical effects. Indeed, the restriction encountered by the flow, when passing through the connecting ducts generates strong shear layers which result in strong velocity gradients and increase the level of turbulence. Turbulence thus generated lasts well beyond the end of the ejection process and helps in promoting flame propagation velocity. Lastly, the hot turbulent jets contain and convey products of partial combustion (active radicals), which spread in the combustion chamber and act as multiple and distributed ignition points. Even though more advanced simulations tool (e.g. LES) are needed to gain an accurate description of the features of the flow leaving the pre-chamber, such as its detailed chemical composition and the cooling and the quenching effects generated by the passage of the flow through the orifices, 3D-CFD RANS simulations remain a valuable tool to globally characterize ignition and combustion patterns. To this extent, a methodology to characterize the three above-mentioned jet features, both from a qualitative and a quantitative perspective is presented.

Fig. 11 displays the evolution of the turbulent kinetic energy, the temperature of the unburned gases, and the OH mass fraction in the main chamber along with the start and the end of the HJE process for the two working points considered so far. Since the mentioned investigation regards the interaction between the pre- and the main chamber with a particular focus on the combustion process, the analysis was performed starting from the time at which the flow goes from the pre-chamber toward the main chamber (−8 CAD aTDCf for both WP#1 and WP#2) and concluded 20 CAD after this event.

Starting from the appearance in the main chamber of the cold turbulent jets, MC mass was assigned to 30 levels (hereinafter also referred to as “bins”) based on the local value of TKE, temperature, and OH mass fraction. Then, the mass that falls inside each bin was then depicted using the colour scale shown in the bottom portion of the illustration. To simplify the reading of the surfaces, the white colour was used to mark empty bins. The lower TKE cut-off value was set to 500 m^2/s^2, which is sufficiently high not to consider any influence of the intake process on the turbulent flow field. Instead, the upper bound was chosen to include up to the most intense turbulences. Regarding the thermal analysis, a temperature range between 650 K and 950 K, representative only of the unburned portion of the main chamber mass was defined and used for this analysis. All the charge assigned to the upper bin has reached a temperature greater than 950 K, a value that, according to the results of the turbulence-chemistry interaction analysis, represents the portion of the mass that is going to be rapidly consumed by the propagating flame front. Finally, OH concentration was used to indicate on one hand the chemical contribution to the main chamber mixture ignition, and on the other hand to assess combustion intensity in the different phases of the ejection process [54]. For these purposes, OH was preferred to other chemical tracers, such as formaldehyde, because the latter disappears behind the flame front, while the concentration of the former shows a maximum in correspondence with the flame front and remains until all the available fuel is completely oxidized. Based on the above, CH_2O provides claims regarding the surface of the flame front, whereas the intermediate species OH is representative of the volume swept by the flame. Upper and lower OH mass fraction thresholds were set to comprehend OH distribution in both stoichiometric and lean operating conditions. The main chamber ignition and combustion process was then subdivided into three distinct phases, which were then used for the subsequent analysis.

1. Ejection of Cold Gases – In the first phase, the pressure difference generated by the pre-chamber combustion pushes the lower part of the pre-chamber charge into the main chamber, generating turbulent, cold, and non-reactive jets. The length of this process is equal to 2.7 CAD in stoichiometric conditions (WP #1) and 3.0 CAD in the lean working point (WP #2). This is due to the slightly lower flame propagation speed observed in lean conditions, which increases the time required by the flame to reach the PC nozzles [32]. Within this temporal frame, the appearance of the turbulent jets leads to the increase of the MC turbulent kinetic energy. However, even though in this stage the maximum pressure difference between the two combustion chambers is observed, since the portion of the combustion chamber interested in the jet development is limited to the near nozzles’ outlet section, only a small portion of the MC mass has reached a TKE level higher than the lower threshold without reaching the maximum value. A sensible difference can be noticed between the two operating conditions. Indeed, in WP #1 the faster PC pressure increment due to combustion (Fig. 9 and Fig. 10) favors the development of high-velocity jets as confirmed by the stronger gradient on the left side of the plot. Even though the temperature of the jets is relatively low, since in this phase the flame is far from the PC nozzle, a minor temperature increase is observed in the MC mass. This is solely because the mixture is compressed since the cold jets’ expulsion begins before the TDC. Finally, from a chemical standpoint, the complete lack of OH radicals reaffirms that cold jets are made up of a mixture of air and fuel that was not involved in any combustion process.
2. Ejection of Hot Gases – In the second phase, PC burnt gases reach the outlet section of the holes, and hot turbulent jets act as both ignition and turbulence sources. Once the main chamber charge has been

ignited, combustion is sustained by jets until the delta pressure between MC and PC goes to zero. The larger pressure difference established between pre- and main chamber, alongside with the high temperature of the jets, increases their energetic content. Even though the length of this process is comparable for the two working points (8.5 CAD), significant differences can be noticed between them. Indeed, the stronger jet intensity observed in WP #1, induces a higher amount of mixture to reach the highest level of TKE for a longer time interval. Moreover, within this phase, a considerable amount of mass features a TKE higher than 500 m^2/s^2 in both operating conditions. There is a small delay between the time at which the peak mass flow rate from PC to MC is measured and between the time at which the maximum amount of MC mass reaches a value higher than 500 m^2/s^2. This is because the jet requires some time to travel across the combustion chamber and induce turbulence on its boundary. From a thermal standpoint, the fraction of the mixture that is incorporated by the high-temperature jets heats up first and then the rest of the charge is warmed through convection. Thanks to two distinct phenomena, in stoichiometric working conditions (WP #1), the temperature rise of the gases starts in advance and with a greater slope. The first contribution is related to the faster penetration of the jets which allows the entrainment of a larger amount of air, especially in the axial direction. In parallel, the higher reactivity of the mixture in stoichiometric conditions supports the advanced development of a flame front on the external boundaries of the jets, which incorporates fresh mixture at higher rates. The reactivity of the hot jets is confirmed by the occurrence of OH radicals in the MC. However, at this stage of the ejection process, the presence of active species is limited to a very small portion. Two main temporal and phenomenological distinctions between the analysed operating conditions can be observed. Indeed, in lean conditions, the stretch to which the flame undergoes when passing through the PC nozzles delays the appearance of the OH radicals of 1 CAD compared to the stoichiometric working point. Second, in accordance with OH chemiluminescence images obtained from optically accessible PC engines [55], OH distribution lies at two different levels in the two operating conditions. A higher mass fraction concentration in the stoichiometric working point and a lower one in the lean operating condition. This means that the flame jet is more stable in stoichiometric conditions, while a reduction in flame intensity and stability is expected as the mixture gets leaner, as confirmed by the CCV reported in Table 3.

3. End of Hot Gases Ejection and Combustion – In the third and last phase, combustion proceeds without being sustained by the ejection of the hot gases, and MC mixture is consumed by the propagation of the turbulent flame front. Even though the ejection process has ended, turbulence intensity still remains quite high thanks to the decay of the most intense turbulences induced by the jets. In stoichiometric conditions, the higher amount of MC mass that had reached the highest TKE level increases the extinction time, as confirmed by the longer right tail (Fig. 11a). In the meantime, a growth in the temperature of the unburned gases can be noticed. This is due to the enlargement of the MC volume that is swept by the hot jets. Moreover, within this phase, the multiple jets merge, consuming the portion of the mixture which was not directly engulfed by the jets. In both operating conditions, the MC mass fraction characterized by a temperature lower than 950 K decreases quickly. In stoichiometric working conditions (WP #1), 65% of the MC mixture has reached a temperature higher than 950 K 20 CAD after the start of the CJE, whereas only 50% in the lean working point (WP #2). From a chemical standpoint, a significant increase in OH concentration is observed within this combustion phase, indicating that a larger amount of MC mixture is affected by combustion phenomena. The rise of the concentration of this active radical concerns a comparable amount of MC mass fraction in the two considered working conditions. Nonetheless, as already seen during the HJE phase, in stoichiometric conditions (WP #1), the higher reactivity of the mixture increases OH concentration, favoring a faster combustion process.

6. Conclusions

In the present work, the comprehensive experimental and 1D/3D-CFD methodology proposed in [32] was exploited to perform numerical analysis on the combustion process of a TJI system. Experimental data were obtained from a single-cylinder, gasoline engine equipped with a passive pre-chamber for a wide range of operating conditions. amongst these two working points at 4000 rpm on the WOT curve, one stoichiometric ($\lambda = 1$) and one lean ($\lambda = 1.2$) were chosen for the current analysis. The 3D-CFD model well correlated with the experimental data and was used to investigate the turbulence-chemistry interaction throughout the entire combustion process and to develop a numerical methodology for describing the propagation of the turbulent jets in the main chamber for different mixtures. The main outcomes can be summarized as follows:

- The interaction between chemistry and turbulence scales plays a crucial role in the development of the combustion process. The enleanment of the mixture increased the velocity scale ratio, thus moving the turbulent combustion regimes toward the broken reaction zone and resulting in a significantly lower flame propagation speed in the PC. Nonetheless, as far as the in-cylinder combustion development is concerned, the small differences captured by the turbulence-chemistry interaction analysis well reflect the similar MC combustion duration. This analysis proved to be a valuable tool for assessing the ignition limit of the mixture under different operating conditions.
- Simplifications introduced by the RANS technique do not allow for a detailed description of the flame-hole interaction, which is known to be one of the most crucial factors in TJI systems. Nonetheless, this approach is capable of providing interesting insights to characterize the MC ignition and combustion processes both from a qualitative and a quantitative standpoint with reduced computational costs. The proposed methodology was able to describe the different stages of the interaction between the two combustion chambers and to capture the main differences between the two working points considered.

The proposed methodology, which combines experimental data with numerical model can pave the way to further research activities with a particular focus on the effects of nozzle hole geometry on PC and MC combustion performances as well as the validation against data gathered from an optically accessible engine.

Declaration of Competing Interest

The authors declare that they have no known competing financial interests or personal relationships that could have appeared to influence the work reported in this paper.

Data availability

The data that has been used is confidential.

References

[1] F. Leach, G. Kalghatgi, R. Stone, P. Miles, The scope for improving the efficiency and environmental impact of internal combustion engines, Transport. Eng. 1 (2020), https://doi.org/10.1016/j.treng.2020.100005.
[2] International Energy Agency, "Net Zero by 2050 - A Roadmap for the Global Energy Sector," 2021.

[3] V. Masson-Delmotte, P. Zhai, H.O. Pörtner, D. Roberts, J. Skea, P.R. Shukla, Global Warming of 1.5 °C: IPCC Special Report On Impacts of Global Warming of 1.5 °C Above Pre-industrial Levels in Context of Strengthening Response to Climate Change, Sustainable Development, and Efforts to Eradicate Poverty, Cambridge University Press, 2022, https://doi.org/10.1017/9781009157940.

[4] European Commission, "'Fit for 55': delivering the EU's 2030 climate target on the way to climate neutrality," 2021.

[5] A. Onorati, R. Payri, B.M. Vaglieco, A.K. Agarwal, C. Bae, G. Bruneaux, M. Canakci, M. Gavaises, M. Günthner, C. Hasse, S. Kokjohn, S.C. Kong, Y. Moriyoshi, R. Novella, A. Pesyridis, R. Reitz, T. Ryan, R. Wagner, H. Zhao, The role of hydrogen for future internal combustion engines, Int. J. Engine Res. 23 (4) (2022) 529–540, https://doi.org/10.1177/14680874221081947.

[6] M. Rottoli, A. Dirnaichner, R. Pietzcker, F. Schreyer, G. Luderer, Alternative electrification pathways for light-duty vehicles in the European transport sector, Transp. Res. D Transp. Environ. 99 (2021), https://doi.org/10.1016/j.trd.2021.103005.

[7] A.G. Abo-Khalil, M.A. Abdelkareem, E.T. Sayed, H.M. Maghrabie, A. Radwan, H. Rezk, A.G. Olabi, Electric vehicle impact on energy industry, policy, technical barriers, and power systems, Int. J. Thermofluids 13 (2022), https://doi.org/10.1016/j.ijft.2022.100134.

[8] G. Kalghatgi, Is it really the end of internal combustion engines and petroleum in transport? Appl. Energy 225 (2018) 965–974, https://doi.org/10.1016/j.apenergy.2018.05.076.

[9] World Energy Council., Global Transport Scenarios 2050, 2004. ISBN 9780946121144.

[10] G. Conway, A. Joshi, F. Leach, A. García, P.K. Senecal, A review of current and future powertrain technologies and trends in 2020, Transport. Eng. 5 (2021), https://doi.org/10.1016/j.treng.2021.100080.

[11] F.A. Ayala, J.B. Heywood, Lean SI engines: the role of combustion variability in defining lean limits, SAE Technical Paper (2007).

[12] F.A. Ayala, M.D. Gerty, J.B. Heywood, Effects of combustion phasing, relative air-fuel ratio, compression ratio, and load on si engine efficiency, SAE Transactions (2006) 177–195.

[13] J. Benajes, R. Novella, J. Gomez-Soriano, P.J. Martinez-Hernandiz, C. Libert, M. Dabiri, Evaluation of the passive pre-chamber ignition concept for future high compression ratio turbocharged spark-ignition engines, Appl. Energy 248 (2019) 576–588, https://doi.org/10.1016/j.apenergy.2019.04.131.

[14] J.M. Desantes, R. Novella, La Morena, J. de, V. Pagano Lng, Achieving ultra-lean combustion using a pre-chamber spark ignition system in a rapid compression-expansion machine, *SAE Technical Papers*, SAE Int. (2019), https://doi.org/10.4271/2019-01-0236.

[15] D. Ju, Z. Huang, X. Li, T. Zhang, W. Cai, Comparison of open chamber and pre-chamber ignition of methane/air mixtures in a large bore constant volume chamber: effect of excess air ratio and pre-mixed pressure, Appl. Energy 260 (2020), https://doi.org/10.1016/j.apenergy.2019.114319.

[16] G. Onofrio, C. Li, P. Garcia Valladolid, J.de La Morena, A. Garcia, P. Tunestal, C. Beatrice, Experimental and numerical assessment of active pre-chamber ignition in heavy duty natural gas stationary engine, *SAE Technical Papers*, SAE Int. (2020), https://doi.org/10.4271/2020-01-0819.

[17] W. Tang, M. Sarathy, Investigate chemical effects of pre-chamber combustion products on main chamber ignition performance under an ultra-lean condition, *SAE Technical Papers*, SAE Int. (2020), https://doi.org/10.4271/2020-01-2001.

[18] A. Shah, P. Tunestal, B. Johansson, Effect of relative mixture strength on performance of divided chamber 'avalanche activated combustion' ignition technique in a heavy duty natural gas engine, *SAE Technical Papers*, SAE Int. (2014), https://doi.org/10.4271/2014-01-1327.

[19] A. Cooper, A. Harrington, M. Bassett, S. Reader, M. Bunce, Application of the passive MAHLE jet ignition system and synergies with miller cycle and exhaust gas recirculation, *SAE Technical Papers*, SAE Int. (2020), https://doi.org/10.4271/2020-01-0283.

[20] J.J. López, R. Novella, J. Gomez-Soriano, P.J. Martinez-Hernandiz, F. Rampanarivo, C. Libert, M. Dabiri, Advantages of the unscavenged pre-chamber ignition system in turbocharged natural gas engines for automotive applications, Energy 218 (2021), https://doi.org/10.1016/j.energy.2020.119466.

[21] J. Benajes, R. Novella, J. Gomez-Soriano, I. Barbery, C. Libert, F. Rampanarivo, M. Dabiri, Computational assessment towards understanding the energy conversion and combustion process of lean mixtures in passive pre-chamber ignited engines, Appl. Therm. Eng. 178 (2020), https://doi.org/10.1016/j.applthermaleng.2020.115501.

[22] G. Onofrio, P. Napolitano, P. Tunestål, C. Beatrice, Combustion sensitivity to the nozzle hole size in an active pre-chamber ultra-lean heavy-duty natural gas engine, Energy 235 (2021), https://doi.org/10.1016/j.energy.2021.121298.

[23] R. Novella, J. Pastor, J. Gomez-Soriano, I. Barbery, C. Libert, F. Rampanarivo, C. Panagiotis, M. Dabiri, Experimental and numerical analysis of passive pre-chamber ignition with EGR and air dilution for future generation passenger car engines, *SAE Technical Papers*, SAE Int. (2020), https://doi.org/10.4271/2020-01-0238.

[24] K. Bardis, G. Xu, P. Kyrtatos, Y.M. Wright, K. Boulouchos, A zero dimensional turbulence and heat transfer phenomenological model for pre-chamber gas engines, *SAE Technical Papers*, SAE Int. (2018), https://doi.org/10.4271/2018-01-1453.

[25] M. Muller, C. Freeman, P. Zhao, H. Ge, in: Numerical simulation of ignition mechanism in the main chamber of a turbulent jet ignition system, Internal Combustion Engine Division, American Society of Mechanical Engineers, 2018, https://doi.org/10.1115/ICEF2018-9587.

[26] E. Mastorakos, P. Allison, A. Giusti, P.de Oliveira, S. Benekos, Y. Wright, C. Frouzakis, K. Boulouchos, Fundamental Aspects of Jet Ignition for Natural Gas Engines, SAE Int. J. Engines 10 (5) (2017) 2429–2438, https://doi.org/10.4271/2017-24-0097.

[27] S. Biswas, S. Tanvir, H. Wang, L. Qiao, On ignition mechanisms of premixed CH4/air and H2/air using a hot turbulent jet generated by pre-chamber combustion, Appl. Therm. Eng. 106 (2016) 925–937, https://doi.org/10.1016/j.applthermaleng.2016.06.070.

[28] R. Novella, J. Gomez-Soriano, I. Barbery, C. Libert, Numerical analysis of the passive pre-chamber ignition concept for light duty applications, Appl. Therm. Eng. 213 (2022), https://doi.org/10.1016/j.applthermaleng.2022.118610.

[29] H. Ge, A.H. Bakir, S. Yadav, Y. Kang, S. Parameswaran, P. Zhao, CFD Optimization of the Pre-Chamber Geometry for a Gasoline Spark Ignition Engine, Front. Mech. Eng. 6 (2021), https://doi.org/10.3389/fmech.2020.599752.

[30] G. Xu, Y.M. Wright, M. Schiliro, K. Boulouchos, Characterization of combustion in a gas engine ignited using a small un-scavenged pre-chamber, Int. J. Engine Res. 21 (7) (2020) 1085–1106, https://doi.org/10.1177/1468087418798918.

[31] M. Silva, X. Liu, P. Hlaing, S. Sanal, E. Cenker, J. Chang, B. Johansson, H.G. Im, Computational assessment of effects of throat diameter on combustion and turbulence characteristics in a pre-chamber engine, Appl. Therm. Eng. 212 (2022), https://doi.org/10.1016/j.applthermaleng.2022.118595.

[32] F. Millo, L. Rolando, A. Piano, P. Sementa, F. Catapano, S.di Iorio, A. Bianco, Experimental and numerical investigation of a passive pre-chamber jet ignition single-cylinder engine, *SAE Technical Papers*, SAE Int. (2021), https://doi.org/10.4271/2021-24-0010.

[33] P. Sementa, F. Catapano, S.Di Iorio, B.M. Vaglieco, Effects of prechamber on efficiency improvement and emissions reduction of a si engine fuelled with gasoline, *SAE Technical Papers*, SAE Int. (2019), https://doi.org/10.4271/2019-24-0236.

[34] W.P. Attard, M. Bassett, P. Parsons, H. Blaxill, A new combustion system achieving high drive cycle fuel economy improvements in a modern vehicle powertrain, in: SAE 2011 World Congress and Exhibition, 2011, https://doi.org/10.4271/2011-01-0664.

[35] P. Chinnathambi, M. Bunce, L. Cruff, RANS based multidimensional modeling of an ultra-lean burn pre-chamber combustion system with auxiliary liquid gasoline injection, SAE Technical Paper (2015), https://doi.org/10.4271/2015-01-0386.

[36] Janas, P. and Niessner, W., "3.2 towards a thermally robust automotive pre-chamber spark plug for turbocharged direct injection gasoline engines".

[37] V. Yakhot, S.A. Orszag, S. Thangam, T.B. Gatski, C.G. Speziale, Development of turbulence models for shear flows by a double expansion technique, Phys. Fluids A 4 (7) (1992) 1510–1520, https://doi.org/10.1063/1.858424.

[38] A. Bianco, F. Millo, A. Piano, Modelling of combustion and knock onset risk in a high-performance turbulent jet ignition engine, Transport. Eng. 2 (2020), https://doi.org/10.1016/j.treng.2020.100037.

[39] F. Millo, L. Rolando, A. Piano, P. Sementa, F. Catapano, S.Di Iorio, A. Bianco, Experimental and numerical investigation of a passive pre-chamber jet ignition single-cylinder engine, *SAE Technical Papers*, SAE Int. (2021), https://doi.org/10.4271/2021-24-0010.

[40] Z. Han, R.D. Reitz. A temperature wall function formulation for variable-density turbulent flows with application to engine convective heat transfer modeling, 1997, https://doi.org/10.1016/0017-9310(96)00117-2.

[41] P.K. Senecal, E. Pomraning, K.J. Richards, T.E. Briggs, C.Y. Choi, R.M. Mcdavid, M. A. Patterson. Multi-dimensional modeling of direct-injection diesel spray liquid length and flam lift-off length using CFD an parallel detailed chemistry, 2003, https://doi.org/10.4271/2003-01-1043.

[42] Convergent Science, "Converge Manual v3.0," 2020.

[43] J. Kim, R. Scarcelli, S. Som, A. Shah, M.S. Biruduganti, D.E. Longman, Assessment of turbulent combustion models for simulating prechamber ignition in a natural gas engine, J. Eng. Gas Turbine Power 143 (9) (2021), https://doi.org/10.1115/1.4050482.

[44] M. Silva CCRC, K. Thuwal, S. Arabia Xinlei Liu CCRC, S. Arabia Ponnya Hlaing CCRC, S.R. Arabia Emre Cenker Aramco, D. Dhahran, S. Arabia James Turner CCRC, S.G. Arabia Hong Im, A computational assessment of combustion submodels for predictive simulations of pre-chamber combustion engines, Proceedings of the ASME (2022).

[45] H.G. Im, M.Ben Houidi, P. Hlaing, F. Almatrafi, Advances in pre-chamber combustion technology for fuel- flexible high-efficiency engines, in: THIESEL 2022 Conference on Thermo- and Fluid Dynamics of Clean Propulsion Powerplants, 2022.

[46] P. Chinnathambi, M. Bunce, L. Cruff, RANS based multidimensional modeling of an ultra-lean burn pre-chamber combustion system with auxiliary liquid gasoline injection, SAE Technical Paper (2015), https://doi.org/10.4271/2015-01-0386.

[47] S.D. Givler, M. Raju, E. Pomraning, P.K. Senecal, N. Salman, R. Reese, Gasoline combustion modeling of direct and port-fuel injected engines using a reduced chemical mechanism, *SAE Technical Papers*, SAE Int. (2013), https://doi.org/10.4271/2013-01-1098.

[48] N. Morgan, A. Smallbone, A. Bhave, M. Kraft, R. Cracknell, G. Kalghatgi, Mapping surrogate gasoline compositions into RON/MON space, Combust. Flame 157 (6) (2010) 1122–1131, https://doi.org/10.1016/j.combustflame.2010.02.003.

[49] Wu, Y., Pal, P., Som, S., and Lu, T., "A skeletal chemical kinetic mechanism for gasoline and gasoline/ethanol blend surrogates for engine CFD applications," 2017.

[50] A. Shah, B. Johansson, CFD simulations of pre-hamber jets' mixing characteristics in a heavy duty natural gas engine, SAE Technical Paper, SAE Int. (2015), 10.4271/2015-01-1890.

[51] N. Peters, Laminar flamelets concepts in turbulent combustion, in: Twenty-First Symposium (International) on Combustion 1231–1250, 1980,, https://doi.org/10.1016/S0082-0784(88)80355-2.
[52] R. Borghi. On the Structure and Morphology of Turbulent Premixed Flames, Springer, Boston, MA, 1985, pp. 117–138, https://doi.org/10.1007/978-1-4684-4298-4_7.
[53] Poinsot, T. and Veynante, D., "Theoretical and numerical combustion," Third Edition, 2012.
[54] Y. Liu, J. Tan, M. Wan, L. Zhang, X. Yao, Quantitative measurement of OH* and CH* chemiluminescence in jet diffusion flames, ACS Omega 5 (26) (2020) 15922–15930, https://doi.org/10.1021/acsomega.0c01093.
[55] Q. Tang, R. Sampath, M. Echeverri Marquez, P. Hlaing, P. Sharma, M.ben Houidi, E. Cenker, J. Chang, G. Magnotti, B. Johansson, Simultaneous negative PLIF and OH* chemiluminescence imaging of the gas exchange and flame jet from a narrow throat pre-chamber, *SAE Technical Papers*, SAE Int. (2020), https://doi.org/10.4271/2020-01-2080.